Cell Calcium. Author manuscript; available in PMC 2017 August 01.

Published in final edited form as:
Cell Calcium. 2017 January ; 61: 22–31. doi:10.1016/j.ceca.2016.10.002.

The mammalian skeletal muscle DHPR has larger Ca^{2+} conductance and is phylogenetically ancient to the early ray-finned fish sterlet (*Acipenser ruthenus*)

Kai Schrötter[#], **Anamika Dayal**[#], and **Manfred Grabner**[*]
Department of Medical Genetics, Molecular and Clinical Pharmacology, Division of Biochemical Pharmacology, Medical University of Innsbruck, Peter Mayr Strasse 1, A-6020, Innsbruck, Austria

[#] These authors contributed equally to this work.

Abstract

The L-type Ca^{2+} channel or dihydropyridine receptor (DHPR) in vertebrate skeletal muscle is responsible for sensing sarcolemmal depolarizations and transducing this signal to the sarcoplasmic Ca^{2+} release channel RyR1 via conformational coupling to initiate muscle contraction. During this excitation-contraction (EC) coupling process there is a slow Ca^{2+} current through the mammalian DHPR which is fully missing in euteleost fishes. In contrast to ancestral evolutionary stages where skeletal muscle EC coupling is still depended on Ca^{2+}-induced Ca^{2+}-release (CICR), it is possible that the DHPR Ca^{2+} conductivity during mammalian (conformational) EC coupling was retained as an evolutionary remnant (vestigiality). Here, we wanted to test the hypothesis that due to the lack of evolutionary pressure in post-CICR species skeletal muscle DHPR Ca^{2+} conductivity gradually reduced as evolution progressed. Interestingly, we identified that the DHPR of the early ray-finned fish sterlet (*Acipenser ruthenus*) is phylogenetically positioned above the mammalian rabbit DHPR which retained robust Ca^{2+} conductivity, but below the euteleost zebrafish DHPR which completely lost Ca^{2+} conductivity. Remarkably, our results revealed that sterlet DHPR still retained the Ca^{2+} conductivity but currents are significantly reduced compared to rabbit. This decrease is due to lower DHPR membrane expression similar to zebrafish, as well as due to reduced channel open probability (P_o). In both these fish species the lower DHPR expression density is partially compensated by higher efficacy of DHPR-RyR1 coupling. The complete loss of P_o in zebrafish and other euteleost species was presumably based on the teleost specific 3rd round of genome duplication (Ts3R). Ts3R headed into the appearance of two skeletal muscle DHPR isoforms which finally, together with the radiation of the euteleost clade, fully lost the P_o.

Keywords

L-Type calcium channel; Skeletal muscle; Sterlet DHPR; Excitation-contraction coupling; Calcium influx evolution

[*]Corresponding author. manfred.grabner@i-med.ac.at (M. Grabner).

1 Introduction

Excitation-contraction (EC) coupling links the electrical excitation of the sarcolemma to the contractile activation of the myofilaments. In vertebrate skeletal muscle, this mechanism depends on the close interplay of the sarcolemmal voltage-gated L-type Ca^{2+} channel or dihydropyridine receptor (DHPR) and the SR Ca^{2+} release channel or ryanodine receptor type-1 (RyR1). Depolarization of the sarcolemma generates conformational changes in the voltage-sensing DHPRα_{1S} subunit [1] which via inter-channel protein – protein interaction opens the RyR1 to release Ca^{2+} from SR stores, required for muscle contraction [2,3]. Simultaneous to this conformational DHPR-RyR1 interaction, there is a small and slowly activating inward Ca^{2+} current through the DHPR, found from lower vertebrates like sharks to higher vertebrates like mammals. The physiological significance of this L-type Ca^{2+} current which is not immediately required for EC coupling [4], is still a matter of uncertainty even after more than 40 years of continuous research [5–7]. In contrast to the skeletal DHPR, activation of the cardiac DHPR isoform leads to a large and rapidly activating inward Ca^{2+} current. Subsequently, this DHPR Ca^{2+} influx triggers opening of the Ca^{2+}-sensitive cardiac ryanodine receptor type-2 (RyR2) to release Ca^{2+} ions from the intracellular SR Ca^{2+} stores. This Ca^{2+}-induced Ca^{2+} release (CICR) mechanism consequently leads to cardiac muscle contraction [8–10].

Very interesting from the phylogenetic view is that the EC coupling mechanism in skeletal muscle fibers of invertebrates and also of early chordates like tunicates or cephalochordates (amphioxus) resembles the cardiac-type EC coupling of vertebrates, since the activation fully depends on external Ca^{2+} influx through the DHPR [11–18]. In skeletal muscles of hagfish and lamprey which are higher up on the phylogenetic tree, conformational (vertebrate skeletal-muscle-type) DHPR-RyR1 coupling is already established [13,19] but maximum force generation still depends on external Ca^{2+} influx [20]. On the evolutionary trajectory to the vertebrates EC coupling became fully Ca^{2+}-influx independent (see Fig. 6 in Ref. [18]). Despite loss of this direct role of Ca^{2+} influx in skeletal muscle EC coupling, robust DHPR currents were recorded from shark muscles [21], which belong to the ancient class “cartilaginous fish” (Chondrichthyes) (Fig. 1). Ca^{2+} influx through the skeletal muscle DHPR continued to exist at least until the phylogenetic branch of the “four limbed vertebrates” (Tetrapods) which is the most successful and species-rich clade within the ancient group of Sarcopterygii (Fig. 1). Finally, evolution led to a complete abolition of DHPR Ca^{2+} influx in the class of “ray-finned fishes” (Actinopterygii), more precisely in their highest developed infraclass of “modern bony fishes” (Euteleostei) containing the model organism zebrafish (*Danio rerio*). Hence, euteleost fish DHPRs fully lost their conductance and solely work as voltage sensors to detect membrane depolarization and as transmitters of this signal to the RyR1 [18]. Therefore, it is very likely that evolutionary replacement of the CICR mechanism in skeletal muscles of early chordates by conformational EC coupling in vertebrates eliminated the evolutionary pressure on the DHPR to conduct Ca^{2+}. Thus, it is feasible that the remaining DHPR Ca^{2+} influx in tetrapods is just an evolutionary remnant (vestigiality) of the ancient CICR stage.

One possibility to reach the state of DHPR non-conductivity in euteleost fishes could be a gradual diminution in conductance during the course of vertebrate phylogeny, due to random

mutations channel regions previously essential for Ca^{2+} conductance. Alternatively, a sharp transition from fully conducting skeletal muscle DHPRs all the way throughout vertebrate phylogeny until a stage of sudden non-conductivity only on the trajectory to the euteleost branch is likewise possible. However, such an abrupt switch would rather suggest novel physiological requirements for DHPR Ca^{2+}-non-conductivity in euteleost fishes, for so far unknown reasons.

To shed light on the mechanism how the complete loss of DHPR Ca^{2+} conductivity in skeletal muscle of euteleost fishes arose – by "fading out" or "switching off" – we investigated DHPR current properties in a selected species, which is evolutionary quite away from the Ca^{2+}-conducting tetrapods but somewhere on the trajectory towards the non-Ca^{2+}-conducting euteleost fishes (Fig. 1). Therefore, we cloned and sequenced the channel-pore-forming DHPRα_{1S} subunit of sterlet (*Acipenser ruthenus*) which is one of the 27 species from the family of sturgeons, close to the basis of Actinopterygii (Fig. 1). Sturgeons, together with the other basal groups, namely bichirs, gars, and bowfins consist of less than 50 extant species and are often considered as "living fossils" since their phylogenetic development has been very slow and their morphology and physiology has remained unchanged since earliest times [22,23]. However, it was unknown if DHPR Ca^{2+} conductivity already disappeared in those early ray-finned fishes.

In the present study, we focused on the biophysical characterization of the skeletal muscle DHPR Ca^{2+} conductivity and EC coupling parameters of sterlet in comparison to the mammalian rabbit (*Oryctolagus cuniculus*) and the euteleost zebrafish (*Danio rerio*). Sterlet DHPRα_{1S} was cloned and expressed in the DHPRα_{1S}-null murine muscle cell line GLT [24]. Interestingly, sterlet DHPRα_{1S} was found to conduct Ca^{2+} currents but at lower expression density and open probability (P_o) compared to the mammalian control DHPR. However, reduced DHPR expression density combined with enhanced DHPR-RyR1 coupling efficacy in sterlet was identical to zebrafish. Overall, our results suggest that DHPR Ca^{2+} conductivity "fades out" on the phylogenetic track from the mammals to euteleost fishes. But the final abrupt "turn off" in euteleost fish was presumably based on an additional extraordinary evolutionary event – the 3rd round of teleost specific genome duplication (Ts3R) at the basis of the teleost branch (Fig. 1). Ts3R led to the emergence of two skeletal muscle DHPRα_{1S} isoforms in teleosts which finally turned non-Ca^{2+} conducting in euteleost fish.

2 Materials and Methods

2.1 Molecular cloning of the sterlet DHPRα_{1S} subunit

Sterlet DHPRα_{1S} subunit (st-α_{1S}) cDNA was created as follows, with nucleotide numbers (nt) given in parentheses and asterisks indicating restriction enzyme (RE) sites introduced by PCR using proofreading Phusion DNA polymerase (Finnzymes reagents). Total RNA from adult sterlet skeletal muscle was isolated using the RNeasy Mini Kit (Qiagen) and reverse transcribed using the Ready-To-Go T-Primed First-Strand Kit (Amersham Pharmacia Biotech). Three cDNA fragments covering the entire open reading frame (ORF) of st-α_{1S} were PCR generated from first-strand cDNA with primers designed according to the zebrafish DHPRα_{1S}-a sequence (GenBank accession no. NM 001146150): SalI*-KpnI (nt

−11 to 1119), KpnI-EcoRI (nt 1119–3004), EcoRI-XbaI* (nt 3004–5643). Two subclones were created by co-ligating fragments SalI*-KpnI (nt −11 to 1119) plus KpnI-EcoRI (nt 1119–3004), as well as ligating fragment EcoRI-XbaI* (nt 3004–5643) into the corresponding polylinker RE sites of pBluescript SK+ (pBS) (Stratagene). For the final construct and N-terminal GFP tagging, excised fragments SalI*-EcoRI (nt −11 to 3004) and EcoRI-XbaI* (nt 3004–5643) were in-frame co-ligated into the SalI/XbaI polylinker RE sites of pGFP^{37} [25]. For an exemplar scheme of the GFP-α_{1S} construct and its expression observed as GFP fluorescence in α_{1S}-null myotubes, see Figs. 1 and 2 of Ref. [25]. After confirming the integrity of the cDNA by sequence analysis (Eurofins MWG Operon, Martinsried, Germany), sterlet DHPRα_{1S} subunit cDNA was deposited in Gen-Bank database (GenBank accession no. HQ636615).

2.2 Expression plasmids

Identical to st-α_{1S}, rabbit and zebrafish DHPRα_{1S} subunits (rb-α_{1S}, zf-α_{1S}-a, and zf-α_{1S}-b, respectively) were N-terminally GFP-tagged by cloning the respective cDNAs into expression plasmid pGFP^{37} as described previously [18,25].

2.3 Zebrafish

Wild-type (wt) zebrafish were bred and maintained under standard laboratory conditions according to the established protocols [31], approved by the Tierethik-Beirat of the Medical University Innsbruck and the Bundesministerium für Wissenschaft und Forschung.

2.4 Culture and transfection of GLT and primary zebrafish myotubes

Murine DHPRα_{1S}-null (GLT) myotubes were cultured on 35-mm culture dishes at 37 °C and 10% CO_2 as described previously [24]. Approximately 4 days after plating, at the onset of myoblast fusion, myotubes were transfected with 1 μg of N-terminally GFP-tagged DHPRα_{1S} cDNA constructs using FuGENE®HD transfection reagent (Promega, Germany). Three to five days after transfection, myotubes were used for whole-cell patch clamp recordings.

Isolation, transfection, and culturing of zebrafish (zf) myotubes were done as described previously [27]. In brief, myoblasts were isolated from 25 to 28 hpf wild-type zebrafish by digesting the tail tissue with collagenase type I (Sigma) and transfected with 2 μg of N-terminally GFP-tagged DHPRα_{1S} cDNA constructs using the AMAXA™ rat neonatal cardiomyocyte nucleofector kit (Lonza, Germany) and plated on 35-mm culture dishes. For whole cell patch clamp recordings myocytes were cultured for 4–6 days at 28 °C.

2.5 Whole cell patch clamp recordings

L-type Ca^{2+} currents in combination with intracellular SR Ca^{2+} release were recorded from transfected (GFP-positive) GLT and primary zf myotubes by loading the cells with the Ca^{2+}-sensitive dye Fluo-4 as described previously in detail [26,27]. Concisely, all recordings were performed at room temperature with an Axopatch 200 B amplifier controlled by the pClamp software. Patch pipettes were fabricated from borosilicate glass (Harvard Instruments) and had resistances of 1.5–2 MΩ for GLT and 3.5–5 MΩ for zf myotubes when filled with the internal solution. Spontaneous contractions of zebrafish myotubes were blocked by adding

100 μM of the myosin-II blocker *N*-benzyl-*p*-toluene sulfonamide (Sigma) to the bath solution. 10 mM Ca^{2+} in the bath solution served as the charge carrier and DHPR Ca^{2+} currents were elicited by 200-ms depolarizing test pulses from a holding potential of −80 mV to test potentials from −50 and +80 mV in 10-mV increments and filtered at 1 kHz and digitized at 5 kHz. To correct for leak currents a P/4 prepulse protocol was employed and to inactivate Na^+ and T-type Ca^{2+} channels a 1-s prepulse to −30 mV was administered before every test pulse. Linear cell capacitance was used to normalize current amplitudes (pA/pF). Following Boltzmann expression was used to fit the current-voltage (I–V) curves:

$$I=G_{max}*(V-V_{rev})/\{1+exp[-(V-V_{1/2})/k_G]\}$$

where I is the current; V is the test potential; V_{rev} is the reversal potential; $V_{1/2}$ is the half maximal activation potential; G_{max} is the maximum channel conductance and k_G is the slope factor.

In parallel to current recordings, the average fluorescence intensity via Fluo-4 fluorescence was measured, normalized to the resting fluorescence and expressed as $\Delta F/F_0$. Following Boltzmann distribution was used to fit the voltage dependence of $\Delta F/F_0$:

$$\Delta F/F_0=(\Delta F/F_0)_{max}/\{1+exp[-(V-V_{1/2})/\mathrm{k}]\}$$

where $V_{1/2}$ is the potential at which $\Delta F/F_0 = (\Delta F/F_0)_{max}/2$ and k is the slope factor.

Recordings were analyzed using ClampFit 9.0 and 10.0 (Axon Instruments) and SigmaPlot 10.0 (SPSS Science, Chicago, IL) software.

2.6 Statistics

Data are reported as mean ± SE. Statistical significance was calculated using unpaired Student's *t* test and p values considered statistically significant are as follows: *, $p < 0.05$; **, $p < 0.01$; and ***, $p < 0.001$.

3 Results

Myotubes of the immortalized murine muscle cell line GLT, lacking DHPRα_{1S} [24], were transfected with expression plasmids encoding either GFP-tagged sterlet DHPRα_{1S} (st-α_{1S}), or GFP-tagged rabbit DHPRα_{1S} (rb-α_{1S}) [25], or a stoichiometric mix of GFP-tagged DHPRα_{1S}-a (from superficial, slow, red muscle) and DHPRα_{1S}-b (from deep, fast, white muscle) of zebrafish (zf-α_{1S}) as controls [18].

3.1 DHPR Ca^{2+} influx into sterlet skeletal muscle is considerably lower compared to mammals

As shown in Fig. 2A, whole cell patch-clamp analysis of GLT myotubes transfected with st-α_{1S} revealed significantly smaller ($p < 0.001$) L-type Ca^{2+} currents (0.6 ± 0.1 pA/pF) compared to rb-α_{1S} transfected cells (2.1 ± 0.2 pA/pF). As expected, zf-α_{1S}-expressing GLT myotubes showed no inward Ca^{2+} currents [18]. Despite the difference in I_{max} between st-

α_{1S} and rb-α_{1S}, no significant difference ($p > 0.05$) in half-maximal current activation potential ($V_{1/2}$) was observed (34.4 ± 2.2 mV and 37.0 ± 1.1 mV for st-α_{1S} and rb-α_{1S}, respectively). Lower membrane expression of st-α_{1S} in the mammalian expression system (GLT) accounting for reduced current density might be due to partial DHPR subunit incompatibilities. An example in this context is the crucial role of the DHPRβ_{1a} subunit in membrane trafficking of DHPRα_{1S} and in the conformational interaction of DHPR and RyR1via tetrad formation [28–31]. Consequently, a putatively weaker interaction between the heterologously expressed fish α_{1S} subunits and the endogenous murine β_{1a} of the GLT myotubes might be responsible for the lower membrane expression of the fish DHPR. To test this, we overexpressed st-α_{1S} as well as the control rb-α_{1S} in primary zebrafish myotubes which completely lack DHPR Ca^{2+} influx (18) and thus serve well as a heterologous expression system for studying Ca^{2+}-conducting DHPR α_{1S} subunits.

However, our results exclude fish/mammalian species-related DHPR subunit incompatibilities, because I_{max} of rb-α_{1S} (8.6 ± 1.3 pA/pF) was again ~3-fold larger compared ($p < 0.01$) to st-α_{1S} (2.9 ± 0.7 pA/pF) (Fig. 2B). Interestingly, however the current size in freshly dissociated zebrafish muscle cells is more than 4-fold higher for both st-α_{1S} and rb-α_{1S} compared ($p < 0.001$) to that obtained from the GLT cell line.

To test whether ~3.5-fold smaller Ca^{2+} currents through st-α_{1S} compared to rb-α_{1S} are due to differences in membrane expression densities rather than biophysical channel properties, we analyzed intramembrane charge movement (Q) at reversal potentials (V_{rev}) upon st-α_{1S} and rb-α_{1S} expression in GLT myotubes (Fig. 3A). At V_{rev} (68.7 ± 0.2 mV for st-α_{1S} and 79.4 ± 1.5 for rb-α_{1S}), maximum of DHPRs are activated with the key advantage that the Q_{rev} signal is not contaminated by inward Ca^{2+} currents. Thus, Q_{rev} recordings provide a convenient measure for the number of functional channels in the membrane [32,33]. As depicted in Fig. 3A, GLT myotubes expressing st-α_{1S} displayed significantly lower ($p < 0.001$) Q_{rev} (2.8 ± 0.5 nC/μF) compared to rb-α_{1S}-expressing myotubes (8.5 ± 0.8 nC/μF), indicating a substantial difference in membrane expression of these two DHPRs. Interestingly, reduction in membrane expression of st-α_{1S} is identical ($p > 0.05$) to that of zf-α_{1S} (2.5 ± 0.2 nC/μF) – the second ray-finned-fish DHPR used in this study, suggesting a fish-specific reduction in DHPR expression density (Fig. 3A).

In addition to the observed reduction in membrane expression, distinct biophysical channel properties might also contribute to smaller Ca^{2+} currents through sterlet DHPR. To test for differences in DHPR channel open probability (P_o), we analyzed the size of the integrated tail currents (Q_{tail}) that emerge after the end of the 200-ms test pulses at V_{rev} upon expression of st-α_{1S}, rb-α_{1S}, or zf-α_{1S} in GLT cells (Fig. 3A; right panel). On plotting Q_{rev} against [$Q_{tail} - Q_{rev}$] the slope of the linear fit provides a convenient index of relative P_o [32,33]. Interestingly, we found a ~3.3-fold smaller slope ($y = 0.77\ x$) and thus lower P_o for st-α_{1S} compared to ($p < 0.01$) rb-α_{1S} ($y = 2.5\ x$; Fig. 3B). As expected, the slope factor of the non-Ca^{2+}-conducting zf-α_{1S} control was around zero. Thus both parameters, reduced membrane expression as well as a lower channel open probability of st-α_{1S} contribute to the reduced DHPR inward Ca^{2+} current in sterlet skeletal muscle.

3.2 Accelerated kinetics of the DHPR Ca^{2+} current in sterlet skeletal muscle

A hallmark of the mammalian skeletal muscle DHPR L-type Ca^{2+} current is its slow activation and inactivation kinetics [34,35]. Interestingly, GLT myotubes expressing st-α_{1S} displayed DHPR currents with significantly ($p < 0.001$) accelerated activation kinetics compared to rb-α_{1S}. As shown in Fig. 4A, the average time to peak measured from I_{max} traces at +40 or +50 mV was 35.1 ± 7.1 ms for st-α_{1S} and 87.2 ± 7.3 ms for rb-α_{1S}. Likewise, DHPR current inactivation, analyzed as fractional inactivation 80 ms after the current peak (R_{80}), was slightly but significantly ($p < 0.01$) enhanced in st-α_{1S} (76.5 ± 3.9%) compared to rb-α_{1S} (88.2 ± 1.7%) (Fig. 4A, right panel). Previously, DHPR transmembrane segment IS3 together with the extracellular linker between transmembrane segments IS3 and IS4 have been identified to be responsible for slow or fast current activation [36,37]. Sequence alignments of this defined region revealed 19 amino acid exchanges between the slow activating rb-α_{1S} and the fast activating st-α_{1S} (Fig. 4B). But, most interestingly, in this region 8 amino acids were identical between st-α_{1S} and the fast cardiac DHPRα_{1C} isoforms, regardless if it was from rabbit (rb-α_{1C}) or garfish (*Lepisosteus oculatus*; gar-α_{1C}). Gars are another ancient order of Actinopterygii, phylogenetically close to the sturgeons (see Fig. 1). We used gar-α_{1C} as a cardiac reference sequence because sterlet α_{1C} sequence is not available so far. However, sterlet cardiac Ca^{2+} currents have been characterized as fast activating and inactivating [38] similar to mammalian cardiac L-type currents [10,36]. Altogether, it appears that the identified amino acid exchanges in the IS3 and IS3-IS4 linker region of st-α_{1S} are responsible for its α_{1C}-type accelerated current activation kinetics.

3.3 Reduced SR Ca^{2+} release but enhanced DHPR – RyR1 coupling efficacy in sterlet skeletal muscle

The conformational change during DHPR activation, measured as charge movement, Q not only opens the DHPR to allow Ca^{2+} influx (except for the teleost zf-α_{1S}), but also leads to the activation of the SR Ca^{2+} release channel, RyR1 via conformational DHPR – RyR1 coupling [3]. Robust intracellular SR Ca^{2+} release in response to 200-ms test pulses from −50 to +70 mV was observed with all the three constructs (Fig. 5A, right panel). However, maximal SR Ca^{2+} release $(\Delta F/F_0)_{max}$ values were significantly lower in GLT myotubes expressing either st-α_{1S} (1.1 ± 0.1; $p < 0.01$) or zf-α_{1S} (1.1 ± 0.1; $p < 0.001$) when compared to rb-α_{1S} (1.8 ± 0.2) (Fig. 5A and B, left graphs). The half-maximum activation potential of Ca^{2+} release ($V_{1/2}$) was identical ($p > 0.05$) for all the three DHPRs (st-α_{1S}, −0.70 ± 1.6 mV; zf-α_{1S}, 0.90 ± 0.8 mV; and rb-α_{1S}, −0.34 ± 1.2 mV).

Next we were interested, if the significant reduction in DHPR charge movement of st-α_{1S} and zf-α_{1S} compared to rb-α_{1S} (Fig. 3) is quantitatively reflected in the observed drop in intracellular SR Ca^{2+} release. To test this, we normalized the $\Delta F/F_0$ values (Fig. 5B, left graphs) to the individual Q_{rev} values (see Fig. 3A). Conversely, normalized graphs (Fig. 5B, right graphs) indicated that the resulting maximal ($\Delta F/F_0/Q_{rev}$) values were significantly higher ($p < 0.001$) in GLT myotubes expressing st-α_{1S} or zf-α_{1S} (0.42 ± 0.04 and 0.38 ± 0.02, respectively) compared to rb-α_{1S} (0.17 ± 0.02). Taken together, these results indicate that DHPR – RyR1 couplons of sterlet and zebrafish skeletal muscles have more than 2-fold enhanced efficacy of SR Ca^{2+} release compared to rabbit.

3.4 Does the “living fossil” sterlet retain a phylogenetically ancient DHPR in skeletal muscle?

Despite surprisingly close similarities between the skeletal muscle DHPRs of the ancestral sterlet and modern teleost zebrafish regarding functional sarcolemmal expression levels and efficient coupling to the SR release channel, there is one fundamental difference between the DHPRs of these two ray-finned fish: Sturgeon DHPR conducts inward Ca^{2+} currents whereas zebrafish DHPR is non-conducting (see Figs. 2 and 3). Previously, we identified crucial single amino acid substitutions (in reference to rb-α_{1S}) responsible for the loss of this Ca^{2+} influx in both zebrafish skeletal muscle DHPR isoforms. In zf-α_{1S}-a the selectivity filter glutamate in repeat I was substituted by glutamine (E303Q) and in zf-α_{1S}-b the neutral asparagine in repeat II, three residues C-terminal to the selectivity filter glutamate, was exchanged to a negatively charged aspartate (N636D) [18]. As displayed in Fig. 6A, in st-α_{1S}, sequences adjacent to the critical selectivity filter glutamates of repeats I–IV are fully homologous to rb-α_{1S} despite the large evolutionary distance between these two different classes – Actinopterygii and Sarcopterygii (see Fig. 1). Hence, any sequence exchange, including the essential substitutions in repeats I and II responsible for Ca^{2+} non-conductivity in teleost fishes, must have evolved within the Actinopterygii, but after the separation of the sturgeon branch.

Even though the central st-α_{1S} selectivity filter region embracing repeats I–IV is 100% homologous to rb-α_{1S}, other areas might be quite heterologous viz., the IS3, IS3-IS4 loop region (see Fig. 4B) and rather share higher homology to zf-α_{1S}, if considering the surprising similarities in DHPR surface expression level and EC coupling efficiency between st-α_{1S} and zf-α_{1S} (see above). Hence, we were interested in the phylogenetic position of st-α_{1S} in comparison to our other two candidate DHPRs, rb-α_{1S} and zf-α_{1S}. So the question arose if the DHPR of the “living fossil” sterlet [22,23] is far the oldest Ca^{2+} channel in this ensemble? If so, are then the similarities in channel properties with the evolutionary most derived euteleost zebrafish rather an analogy than the manifestation of evolutionary closeness? To this aim, we calculated a phylogenetic tree based on parsimony analysis of full-length amino acid sequence alignments of rb-α_{1S}, st-α_{1S}, and zf-α_{1S} together with the cardiac DHPR counterparts (Fig. 6B). Ancestral DHPR isoforms from housefly *Musca domestica* [39] and the tunicate *Halocynthia roretzi* [40] were used as outgroups. Strikingly, the mammalian rb-α_{1S} emerges as the ancestral skeletal muscle DHPR, with st-α_{1S} in-between and the two zf-α_{1S} paralogs as the phylogenetically most derived. We see a similar picture in the clade comprising the cardiac DHPRs. The mammalian isoform, rb-α_{1C} is basic to the cardiac DHPRs of both actinopterygian species.

4 Discussion

To shed light on a fascinating phenomenon of muscle physiology – the loss of skeletal muscle DHPR Ca^{2+} influx during vertebrate evolution, we performed sequence comparisons, phylogenetic tree analysis, and patch-clamp electrophysiology on three phylogenetically distant skeletal muscle DHPRs in this study.

4.1 Phylogenetically most derived DHPRs in skeletal muscles of the euteleost zebrafish

Previously, we detected that zebrafish has not only two isoforms of the DHPRα_{1S} subunit, but most interestingly that both paralogs implemented Ca^{2+}-non-conductivity by different point mutations leading to distinct molecular strategies of Ca^{2+} blockade [18]. Additionally, we showed that all tested euteleost DHPRα_{1S} isoforms carried amino acid substitutions that prevented Ca^{2+} influx in skeletal muscle. Remarkably, on the basis of the teleost branch in the order Osteoglossiformes (see Fig. 1), DHPRα_{1S} already exist in two paralogs, but the amino acid exchanges essential for blocking the Ca^{2+} influx did not take place yet [18].

Teleost fishes are by far the highest derived clade in the class of Actinopterygii and the most diversified and dominant group among vertebrates with over 30,000 species, which is approximately equal to all other vertebrate groups combined [41]. A vast majority of them (>95%) belong to the highest developed Euteleostei, which are certainly the most successful vertebrate group, probably due to their rich gene supply as a result of the 3rd teleost specific genome duplication (Ts3R, see Fig. 1) in this lineage [23]. Interestingly, alone this fact means that half of the vertebrate species possess non-Ca^{2+}-conducting skeletal muscle DHPRs which exemplifies that “silencing” of skeletal muscle DHPRs is in no case a marginal phenomenon. Hence, in this study we choose as the first of three model organisms, the euteleost zebrafish (*Danio rerio*) as the canonical vertebrate species with non-Ca^{2+} conducting skeletal muscle DHPR (see Fig. 1).

4.2 The skeletal muscle DHPR of sterlet is Ca^{2+} conducting

Sterlet (*Acipenser ruthenus*) from the family of sturgeons, with unknown DHPR Ca^{2+} -conductivity status and with its position at the basis of the Actinopterygii phylogenetically sufficiently distant to the euteleost zebrafish, was selected as the second model organism. Sturgeons belong to an ancient clade which separated from the other ray-finned fishes around 360 million years ago and thus are phylogenetically located far below the teleosts [18,42–45]. As mentioned above, sturgeons together with the other basal actinopterygian (bichirs, gars, and bowfins) are often considered as “living fossils” with very slow phylogenetic development and apparently stagnating morphological and physiological advances [22,23]. However, due to the lack of biophysical studies on skeletal muscle DHPRs of these early ray-finned fishes, it was unknown if DHPR Ca^{2+} conductivity was existing or rather lost due to the lack of evolutionary pressure since the stages of earliest vertebrates (see Introduction). Finally, our present study provides clear evidence that sturgeons (and consequently also the clade phylogenetically beneath – the bichirs) possess Ca^{2+}-conducting DHPRs in skeletal muscle.

4.3 The mammalian DHPR is evolutionary ancient to sterlet and zebrafish

The third model organism in this study is the mammalian species rabbit (*Oryctolagus cuniculus*), which is archetypical for a Ca^{2+}-conducting skeletal muscle DHPR [46]. Rabbit DHPRα_{1S} shares similar amino acid sequence identity to the representatives (n = 11) of different mammalian families, ranging from 89% (African elephant), 93% (human, mouse, rat, cat, and horse) to 94% (walrus). Mammals are a clade within the tetrapods which evolved around 390 million years ago [47] as the most advanced branch from the evolutionary less successful (because most species are extinct) second class of “bony fishes”

(Osteichtyes), the so called “lobe-finned fishes” (Sarcopterygii) (Fig. 1). Since skeletal muscle DHPRs of amphibians [48,49], birds [50], and mammals [46,51] were characterized to conduct Ca^{2+}, we can unequivocally conclude that also their ancestors, and thus the entire clade of Sarcopterygii, embraces species with Ca^{2+}-conducting DHPRs.

Surprisingly, our phylogenetic and biophysical analyses revealed that the mammalian rabbit not only possesses DHPRs (skeletal muscle as well as cardiac) that are evolutionary ancient to both selected actinopterygian DHPRs (Fig. 6), but also that only the rabbit skeletal muscle DHPR produces a robust inward Ca^{2+} current. Thus, skeletal and cardiac muscle DHPRs of the so called “living fossil” sterlet are phylogenetically at a more derived position compared to corresponding rabbit isoforms. DHPR Ca^{2+} influx in sterlet is significantly reduced compared to rabbit (see Fig. 2), which in addition underlines the more advanced evolutionary stage and accordingly supports the hypothesis of a gradual disappearance of skeletal muscle DHPR Ca^{2+} conductance during vertebrate evolution. Interestingly, the reduction of Ca^{2+} conductance of sterlet DHPR is based on two mechanisms: (i) lower membrane expression and (ii) lower open probability (P_o) of the channel. Lower DHPR surface expression in sterlet already anticipates the reduced DHPR expression found in the euteleost zebrafish. But in contrast to sterlet, P_o of the zebrafish DHPR already reached the zero level (see Fig. 3). However, it is likewise possible that single channel conductance (γ) or both single channel parameters, P_o and γ, are reduced in sterlet. Remarkably, this drop in DHPR surface expression is not 1:1 reflected in lower intracellular Ca^{2+} release, as might be expected from a lower number of actively interacting DHPR-RyR1 couplons. Our results reveal that both, sterlet DHPR as well as the most derived zebrafish DHPR possess higher DHPR-RyR coupling efficacy which partially compensates for the lower DHPR membrane expression.

Another interesting aspect of this study is that the current through the sterlet DHPR does not follow the archetypical skeletal muscle L-type current kinetics. Instead of activating and inactivating in a slow mode, it is significantly faster in both aspects to all the so far described skeletal muscle DHPRs [46,48–51]. Consequently, whereas the reduced size of the sterlet DHPR current points to a more advanced evolutionary state (supported by the pedigree in Fig. 6), the fast current kinetics resembles rather the phylogenetically ancient cardiac isoform. Additionally, the 8 amino acids of cardiac sequence retained in transmembrane segment IS3 and the adjacent IS3-IS4 linker, considered to be responsible for the fast activation kinetics, seems to present an interesting atavism.

4.4 The loss of DHPR Ca^{2+} conductance in Euteleostei – fading out or switching off?

The answer to our primary question, if the complete loss of DHPR Ca^{2+} conductance in skeletal muscle of euteleost fishes emerged by slowly “fading out” due to the lack of evolutionary pressure or rather was “switched off” due to e.g., new muscle-physiological concepts (see above), appears to be bilateral. Still existent but considerably lower Ca^{2+} influx in sterlet, a species that is phylogenetically (see Fig. 1) and also in terms of DHPR evolution (see Fig. 6) located between rabbit and zebrafish, strongly suggests a steady loss of Ca^{2+} conductance during vertebrate evolution. However, the final abrupt “switch off” needed an extraordinarily evolutionary event, the Ts3R, which occurred at the base of the

teleost radiation [23,52] (Fig. 1). The significance of whole-genome duplications (WGDs) for shaping the architecture of vertebrate genomes, yielding vast biological diversity and hence evolutionary success, are widely accepted and increasing evidences for two rounds of WGDs (1R and 2R) at the basis of vertebrate radiation as well as a 3rd WGD (Ts3R) at the basis of the teleost clade (see Fig. 1) emerged in recent years [23,52–57]. Numerous crucial progresses in muscle evolution are known to originate from 1R- and 2R-duplications. One was the differentiation of muscle-specific myosin II into cardiac and skeletal muscle isoforms [13,55,58]. Similarly, the diversification of the Ca^{2+} release channel into RyR1 and RyR2 [59] and of DHPRα_1 into DHPRα_{1S} and DHPRα_{1C} occurred, allowing the acquisition of direct DHPRα_{1S}-RyR1 interaction in skeletal muscle in parallel to the ancient DHPRα_{1C}-RyR2 CICR mechanism still persisting in cardiac muscle [16]. DHPRα_{1S} isoforms evolved to a considerably higher degree compared to DHPRα_{1C} (Fig. 6), pointing to a tighter selection pressure on DHPRα_{1S} due to the requirement to develop efficient conformational EC coupling. Finally, Ts3R led to splitting of DHPRα_{1S} into DHPRα_{1S}-a and DHPRα_{1S}-b isoforms in teleosts, specific for slow and fast skeletal muscles, respectively [18]. Amino acid substitutions induced by this new round of DHPRα_{1S} isoform formation, together with the silencing of both DHPRs led to by far the most derived DHPRα_{1S} isoforms on the phylogenic tree, with the fast muscle DHPRα_{1S}-b at the topmost position (Fig. 6).

One possible physiological conception for this obvious final “enforcement” of DHPR non-Ca^{2+}-conductivity following DHPRα_{1S} duplication during Ts3R might involve adaptations in the cellular energy management. Thus, the block of Ca^{2+} influx during EC coupling abolishes the need for Ca^{2+} extrusion from the myoplasm, allowing a pure Ca^{2+} recycling pathway between the myoplasm and internal SR Ca^{2+} stores. This ATP-saving concept might be of special relevance in the poikilothermic teleosts but would play only a minor role in mammals where a constant basal metabolic activity of skeletal muscles is nonetheless required for heat production for maintenance of a stable body temperature. To test this hypothesis swim tunnel respirometry experiments [60] on a transgenic zebrafish strain expressing a Ca^{2+} conducting DHPR in skeletal muscle are on the way.

5 Conclusion

Biophysical and phylogenetic analyses of the skeletal muscle DHPR of the early ray-finned fish species sterlet (*Acipenser ruthenus*) support the hypothesis that DHPR Ca^{2+} conductivity “fades out” during vertebrate evolution due to the lack of evolutionary pressure on this presumably vestigial current. This conclusion is drawn from the significantly lower open probability (P_o) of the phylogenetically derived sterlet DHPR when compared to the relatively ancestral mammalian rabbit DHPR. However, the final “turn off” of DHPR Ca^{2+}-conductivity did not take place before the stage of euteleost fishes. Radiation of this clade was preceded by the teleost-specific 3rd round of whole genome duplication, Ts3R. Consequently, different amino acid substitutions in the duplicated DHPRα_{1S} isoforms enforced the complete block of DHPR Ca^{2+}-conductivity in euteleost fishes.

Europe PMC Funders Author Manuscripts

Acknowledgements

The authors thank Birgit Kagerbauer for excellent technical help. This work was supported by the Austrian Science Fund (FWF; grants P23229-B09 and P27392-B21, and graduate program DK-W1101-B12 to M.G.)

Abbreviations

EC	excitation-contraction
DHPR	dihydropyridine receptor
RyR1	ryanodine receptor type-1
SR	sarcoplasmic reticulum
CICR	Ca^{2+}-induced Ca^{2+} release
GLT	immortalized DHPRα_{1S}-null murine myotubes
P_o	open probability
Ts3R	teleost-specific 3rd round of genome duplication
st-α_{1S}	sterlet DHPR α_{1S} subunit
rb-α_{1S}	rabbit DHPR α_{1S} subunit
zf-α_{1S}	zebrafish DHPR α_{1S} subunit
GFP	green fluorescent protein
nt	nucleotide numbers.

References

[1]. Tanabe T, Takeshima H, Mikami A, et al. Primary structure of the receptor for calcium channel blockers from skeletal muscle. Nature. 1987; 328:313–318.

[2]. Schneider MF, Chandler WK. Voltage dependent charge movement of skeletal muscle: a possible step in excitation-contraction coupling. Nature. 1973; 242:244–246. [PubMed: 4540479]

[3]. Rios E, Brum G. Involvement of dihydropyridine receptors in excitation-contraction coupling in skeletal muscle. Nature. 1987; 325:717–720.

[4]. Armstrong CM, Bezanilla FM, Horowicz P. Twitches in the presence of ethylene glycol bis(-aminoethyl ether)-N,N'-tetracetic acid. Biochim Biophys Acta. 1972; 267:605–608. [PubMed: 4537984]

[5]. Dirksen RT. Checking your SOCCs and feet: the molecular mechanisms of Ca^{2+} entry in skeletal muscle. J Physiol. 2009; 587:3139–3147. [PubMed: 19406875]

[6]. Beam KG, Bannister RA. Looking for answers to EC coupling's persistent questions. J Gen Physiol. 2010; 136:7–12. [PubMed: 20584887]

[7]. Bannister RA, Beam KG. Ca_V 1.1: The atypical prototypical voltage-gated Ca^{2+} channel. Biochim Biophys Acta. 2013; 1828:1587–1597. [PubMed: 22982493]

[8]. Reuter H, Beeler GW Jr. Calcium current and activation of contraction in ventricular myocardial fibers. Science. 1969; 163:399–401. [PubMed: 5762779]

[9]. Nabauer M, Callewaert G, Cleemann L, Morad M. Regulation of calcium release is gated by calcium current not gating charge, in cardiac myocytes. Science. 1989; 244:800–803. [PubMed: 2543067]

[10]. Tanabe T, Mikami A, Numa S, Beam KG. Cardiac-type excitation-contraction coupling in dysgenic skeletal muscle injected with cardiac dihydropyridine receptor cDNA. Nature. 1990; 344:451–453. [PubMed: 2157159]

[11]. Hagiwara S, Henkart MP, Kidokoro Y. Excitation contraction coupling in Amphioxus muscle cells. J Physiol. 1971; 219:233–251. [PubMed: 5158596]

[12]. Scheuer T, Gilly WF. Charge movement and depolarisation-contraction coupling in arthropod vs. vertebrate skeletal muscle. Proc Natl Acad Sci U S A. 1986; 83:8799–8803. [PubMed: 2430301]

[13]. Inoue I, Tsutsui I, Bone Q, Brown ER. Evolution of skeletal muscle excitation-contraction coupling and the appearance of dihydropyridine-sensitive intramembrane charge movement. Proc R Soc Lond B: Biol Sci. 1994; 255:181–187.

[14]. Takekura H, Franzini-Armstrong C. The structure of Ca^{2+} release units in arthropod body muscle indicates an indirect mechanism for excitation-contraction coupling. Biophys J. 2002; 83:2742–2753. [PubMed: 12414707]

[15]. Okamura Y, Izumi-Nakaseko H, Nakajo K, Ohtsuka Y, Ebihara T. The ascidian dihydropyridine-resistant calcium channel as the prototype of chordate L-type calcium channel. Neurosignals. 2003; 12:142–158. [PubMed: 12904687]

[16]. Di Biase V, Franzini-Armstrong C. Evolution of skeletal type e-c coupling: a novel means of controlling calcium delivery. J Cell Biol. 2005; 171:695–704. [PubMed: 16286507]

[17]. Collet C. Excitation-contraction coupling in skeletal muscle fibers from adult domestic honeybee. Pflugers Arch. 2009; 458:601–612. [PubMed: 19198873]

[18]. Schredelseker J, Shrivastav M, Dayal A, Grabner M. Non-Ca^{2+}-conducting Ca^{2+} channels in fish skeletal muscle excitation-contraction coupling. Proc Natl Acad Sci U S A. 2010; 107:5658–5663. [PubMed: 20212109]

[19]. Inoue I, Tsutsui I, Bone Q. Excitation-contraction coupling in skeletal and caudal heart muscle of the hagfish *Eptatretus burgeri* Girard. J Exp Biol. 2002; 205:3535–3541. [PubMed: 12364406]

[20]. Nasledov GA, Katina IE, Zhitnikova Iu V. Characteristics of functioning of electromechanical coupling in striated muscles of higher and lower vertebrates. Biofizika. 2002; 47:716–727. [PubMed: 12298213]

[21]. Rogers CM, Brown ER. Differential sensitivity to calciseptine of L-type Ca^{2+} currents in a 'lower' vertebrate (*Scyliorhinus canicula*), a protochordate (*Branchiostoma lanceolatum*) and an invertebrate (*Alloteuthis subulata*). Exp Physiol. 2001; 86:689–694. [PubMed: 11698962]

[22]. Krieger J, Fuerst PA. Evidence for a slowed rate of molecular evolution in the order Acipenseriformes. Mol Biol Evol. 2002; 19:891–897. [PubMed: 12032245]

[23]. Meyer A, Van de Peer Y. From 2R to 3R: evidence for a fish-specific genome duplication (FSGD). Bioessays. 2005; 27:937–945. [PubMed: 16108068]

[24]. Powell JA, Petherbridge L, Flucher BE. Formation of triads without the dihydropyridine receptor alpha subunits in cell lines from dysgenic skeletal muscle. J Cell Biol. 1996; 134:375–387. [PubMed: 8707823]

[25]. Grabner M, Dirksen RT, Beam KG. Tagging with green fluorescent protein reveals a distinct subcellular distribution of L-type and non-L-type Ca^{2+} channels expressed in dysgenic myotubes. Proc Natl Acad Sci U S A. 1998; 95:1903–1908. [PubMed: 9465115]

[26]. Weiss RG, O'Connell KMS, Flucher BE, et al. Functional analysis of the R1086H malignant hyperthermia mutation in the DHPR reveals an unexpected influence of the III-IV loop on skeletal muscle EC coupling. Am J Physiol Cell Physiol. 2004; 287:C1094–C1102. [PubMed: 15201141]

[27]. Schredelseker J, Dayal A, Schwerte T, Franzini-Armstrong C, Grabner M. Proper restoration of excitation-contraction coupling in the dihydropyridine receptor β_1 -null zebrafish *relaxed* is an exclusive function of the β_{1a} subunit. J Biol Chem. 2009; 284:1242–1251. [PubMed: 19008220]

[28]. Schredelseker J, Di Biase V, Obermair GJ, Felder TE, Flucher BE, Franzini-Armstrong C, Grabner M. The β_{1a} subunit is essential for the assembly of dihydropyridine-receptor arrays in skeletal muscle. Proc Natl Acad Sci U S A. 2005; 102:17219–17224. [PubMed: 16286639]

[29]. Dolphin AC. Calcium channel auxiliary alpha2delta and beta subunits: trafficking and one step beyond. Nat Rev Neurosci. 2012; 13:542–555. [PubMed: 22805911]

[30]. Simms BA, Zamponi GW. Trafficking and stability of voltage-gated calcium channels. Cell Mol Life Sci. 2012; 69:843–856. [PubMed: 21964928]

[31]. Dayal A, Bhat V, Franzini-Armstrong C, Grabner M. Domain cooperativity in the β_{1a} subunit is essential for dihydropyridine receptor voltage sensing in skeletal muscle. Proc Natl Acad Sci U S A. 2013; 110:7488–7493. [PubMed: 23589859]

[32]. Wei X, Neely A, Lacerda AE, et al. Modification of Ca^{2+} channel activity by deletions at the carboxyl terminus of the cardiac alpha 1 subunit. J Biol Chem. 1994; 269:1635–1640. [PubMed: 7507480]

[33]. Takahashi SX, Miriyala J, Colecraft HM. Membrane-associated guanylate kinase-like properties of β-subunits required for modulation of voltage-dependent Ca^{2+} channels. Proc Natl Acad Sci U S A. 2004; 101:7193–7198. [PubMed: 15100405]

[34]. Bean BP. Classes of calcium channels in vertebrate cells. Annu Rev Physiol. 1989; 51:367–384. [PubMed: 2540697]

[35]. Tsien RW, Lipscombe D, Madison DV, Bley KR, Fox AP. Multiple types of neuronal calcium channels and their selective modulation. Trends Neurosci. 1988; 11:431–438. [PubMed: 2469160]

[36]. Nakai J, Adams BA, Imoto K, Beam KG. Critical roles of the S3 segment and S3-S4 linker of repeat I in activation of L-type calcium channels. Proc Natl Acad Sci U S A. 1994; 91:1014–1018. [PubMed: 8302825]

[37]. Tuluc P, Benedetti B, Coste de Bagneaux P, Grabner M, Flucher BE. Two distinct voltage-sensing domains control voltage sensitivity and kinetics of current activation in Ca_V 1.1 calcium channels. J Gen Physiol. 2016; 147:437–449. [PubMed: 27185857]

[38]. Haworth TE, Haverinen J, Shiels HA, Vornanen M. Electrical excitability of the heart in a Chondrostei fish, the Siberian sturgeon (*Acipenser baerii*). Am J Physiol Regul Integr Comp Physiol. 2014; 307:R1157–R1166. [PubMed: 25163915]

[39]. Grabner M, Bachmann A, Rosenthal F, et al. Insect calcium channels. Molecular cloning of an alpha1-subunit from housefly (*Musca domestica*) muscle. FEBS Lett. 1994; 339:189–194. [PubMed: 8313972]

[40]. Okagaki R, Izumi H, Okada T, Nagahora H, Nakajo K, Okamura Y. The maternal transcript for truncated voltage-dependent Ca^{2+} channels in the ascidian embryo: a potential suppressive role in Ca^{2+} channel expression. Dev Biol. 2001; 230:258–277. [PubMed: 11161577]

[41]. Volff JN. Genome evolution and biodiversity in teleost fish. Heredity (Edinb). 2005; 94:280–294. [PubMed: 15674378]

[42]. Laurin M, Reisz RR. A reevaluation of early amniote phylogeny. Zool J Linn Soc. 1995; 113:165–223.

[43]. Steinbacher P, Haslett JR, Sanger AM, Stoiber W. Evolution of myogenesis in fish: a sturgeon view of the mechanisms of muscle development. Anat Embryol (Berl). 2006; 211:311–322. [PubMed: 16506067]

[44]. Near TJ, Eytan RI, Dornburg A, et al. Resolution of ray-finned fish phylogeny and timing of diversification. Proc Natl Acad Sci U S A. 2012; 109:13698–13703. [PubMed: 22869754]

[45]. Betancur-R R, Broughton RE, Wiley EO, et al. The Tree of Life and a New Classification of Bony Fishes. PLOS Currents Tree of Life (1st ed). 2013

[46]. Tanabe T, Beam KG, Powell JA, Numa S. Restoration of excitation-contraction coupling and slow calcium current in dysgenic muscle by dihydropyridine receptor complementary DNA. Nature. 1988; 336:134–139. [PubMed: 2903448]

[47]. Narkiewicz K, Narkiewicz M. The age of the oldest tetrapod tracks from Zachelmie, Poland. Lethaia Focus. 2015; 48:10–12.

[48]. Cota G, Nicola Siri L, Stefani E. Calcium-channel gating in frog skeletal muscle membrane: effect of temperature. J Physiol. 1983; 338:395–412. [PubMed: 6308247]

[49]. Sanchez JA, Stefani E. Kinectic properties of calcium channels of twitch muscle fibres of the frog. J Physiol. 1983; 337:1–17. [PubMed: 6308234]

[50]. Trujillo X, Huerta M, Vásquez C, Andrade F. Adrenaline diminishes K^+ contractures and Ba^{2+} current in chicken slow skeletal muscle fibres. J Muscle Res Cell Motil. 2002; 23:157–165. [PubMed: 12416722]

[51]. Beam KG, Knudson CM. Calcium currents in embryonic and neonatal mammalian skeletal muscle. J Gen Physiol. 1988; 91:781–798. [PubMed: 2458429]

[52]. Glasauer SM, Neuhauss SC. Whole-genome duplication in teleost fishes and its evolutionary consequences. Mol Genet Genomics. 2014; 289:1045–1060. [PubMed: 25092473]

[53]. Sidow A. Gen(om)e duplications in the evolution of early vertebrates. Curr Opin Genet Dev. 1996; 6:715–722. [PubMed: 8994842]

[54]. Holland PW. More genes in vertebrates. J Struct Funct Genomics. 2003; 3:75–84. [PubMed: 12836687]

[55]. McGuigan K, Phillips PC, Postlethwait JH. Evolution of sarcomeric myosin heavy chain genes: evidence from fish. Mol Biol Evol. 2004; 21:1042–1056. [PubMed: 15014174]

[56]. Storz JF, Opazo JC, Hoffmann FG. Gene duplication, genome duplication, and the functional diversification of vertebrate globins. Mol Phylogenet Evol. 2013; 66:469–478. [PubMed: 22846683]

[57]. Plata G, Vitkup D. Genetic robustness and functional evolution of gene duplicates. Nucleic Acids Res. 2014; 42:2405–2414. [PubMed: 24288370]

[58]. Franzini-Armstrong C, Protasi F, Ramesh V. Shape, size, and distribution of Ca^{2+} release units and couplons in skeletal and cardiac muscles. Biophys J. 1999; 77:1528–1539. [PubMed: 10465763]

[59]. Chugun A, Taniguchi K, Murayama T, et al. Subcellular distribution of ryanodine receptors in the cardiac muscle of carp (*Cyprinus carpio*). Am J Physiol Regul Integr Comp Physiol. 2003; 285:R601–609. [PubMed: 12805094]

[60]. Tudorache C, Burgerhout E, Brittijn S, van den Thillart G. Comparison of swimming capacity and energetics of migratory European eel (*Anguilla anguilla*) and New Zealand short-finned eel (*A. australis*). Front Physiol. 2015; 6:256. [PubMed: 26441675]

[61]. Zhu M, Yu X, Ahlberg PE, et al. A Silurian placoderm with osteichthyan-like marginal jaw bones. Nature. 2013; 502:188–193. [PubMed: 24067611]

[62]. Hoegg S, Brinkmann H, Taylor JS, Meyer A. Phylogenetic timing of the fish-specific genome duplication correlates with phenotypic and taxonomic diversification in fishes. J Mol Evol. 2004; 59:190–203. [PubMed: 15486693]

[63]. Van de Peer Y, Maere S, Meyer A. The evolutionary significance of ancient genome duplications. Nat Rev Genet. 2009; 10:725–732. [PubMed: 19652647]

[64]. Maddison DR, Schulz K-S, Maddison WP. The Tree of Life Web ProjectZootaxa. Zootaxa. 2007; 1668:1–766.

[65]. Wu J, Yan Z, Li Z, et al. Structure of the voltage-gated calcium channel Ca_V 1.1 complex. Science. 2015; 350:23951–23959.

Europe PMC Funders Author Manuscripts

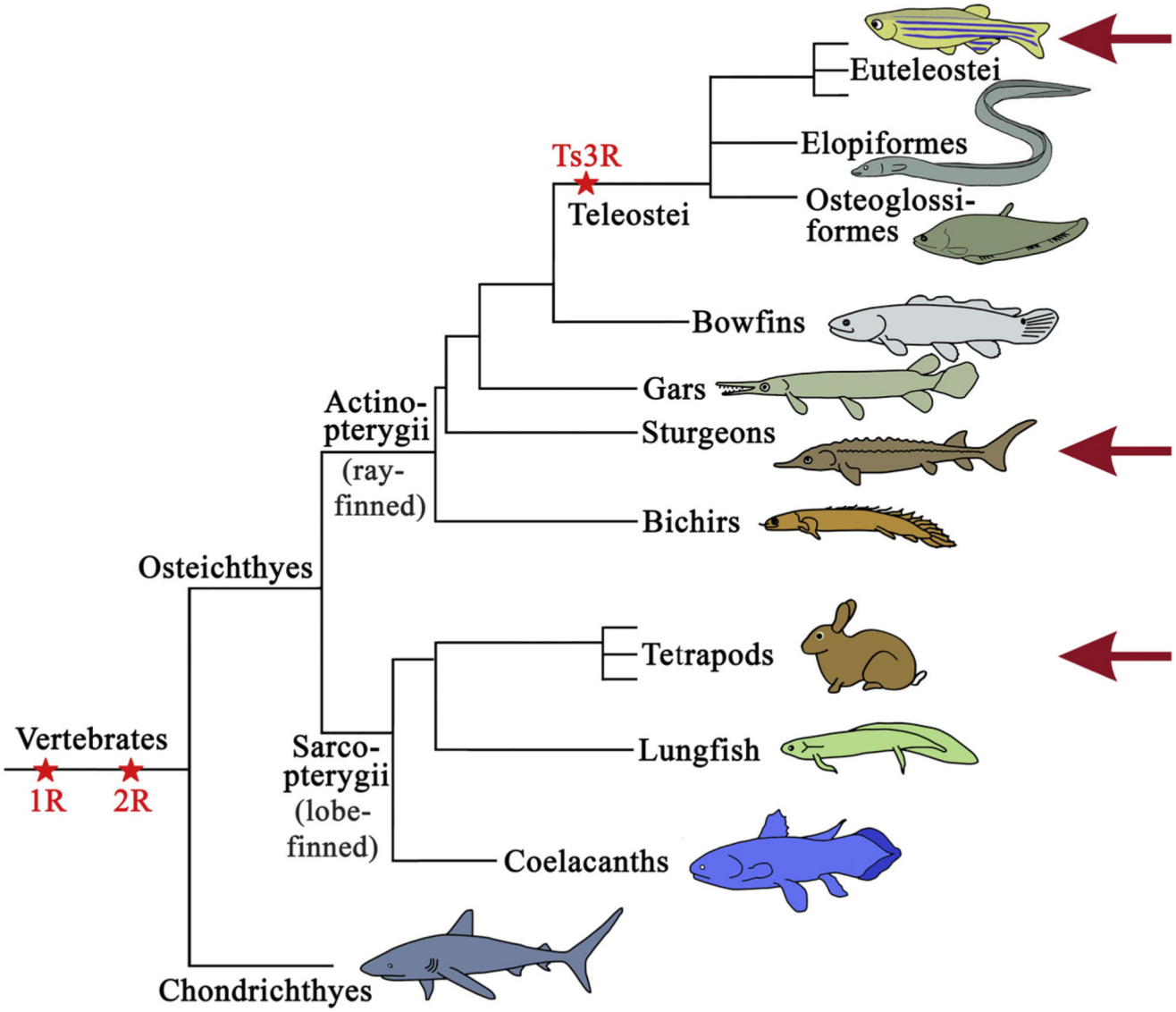

Fig. 1.

Vertebrate phylogeny and positions of the three species examined in the study. Phylogenetic relationship between the major lineages of actinopterygian (ray-finned) fishes and sarcopterygian (lobe-finned) fishes, including tetrapods as direct descendants of this clade. A single sister group to the Osteichthyes (bony fishes) are the Chondrichthyes (cartilaginous fishes; including sharks, rays, and chimaeras) [61]. Whole genome duplications (WGDs) are indicated by red asterisks, with the first two rounds (1R and 2R) at the vertebrate stem and the teleost-specific third round (Ts3R) at the basis of the teleost radiation [23,62,63]. Red arrows indicate the phylogenic status of the three species – rabbit, sterlet, and zebrafish examined in the study. Phylogenetic tree is drawn after the Tree of Life web project [64]. Part of animal outlines was modified from [18]. (For interpretation of the references to colour in this figure legend, the reader is referred to the web version of this article.)

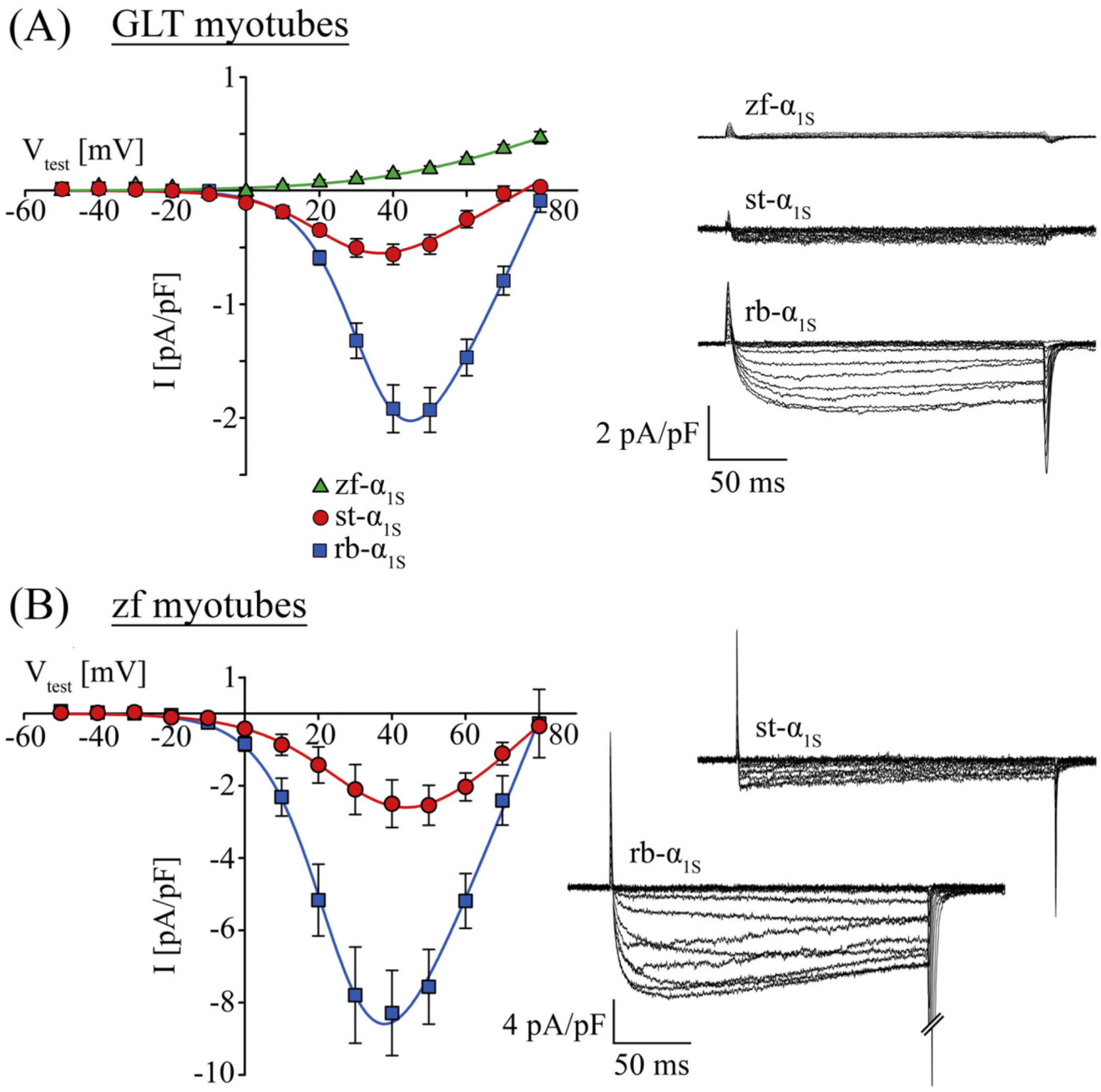

Fig. 2.

DHPR Ca^{2+} currents are smaller in sterlet than in rabbit skeletal muscle. (A) GLT myotubes transfected with st-α_{1S} (red circles; n = 20) expressed substantial DHPR currents, but significantly lower ($p < 0.001$) than rb-α_{1S} expressing myotubes (blue squares; n = 28). Control recordings with zf-α_{1S} (green diamonds; n = 19) displayed the expected lack of inward Ca^{2+} currents [18]. (B) Overexpression of st-α_{1S} (n = 6) or rb-α_{1S} (n = 12) in zebrafish (zf) myotubes showed in general, a higher current density but again a significant ($p < 0.01$) difference of similar dimension like observed in GLT myotubes. Representative

Europe PMC Funders Author Manuscripts

current traces are shown on the right and current-voltage (*I–V*) graphs on the left. (For interpretation of the references to colour in this figure legend, the reader is referred to the web version of this article.)

Europe PMC Funders Author Manuscripts

Europe PMC Funders Author Manuscripts

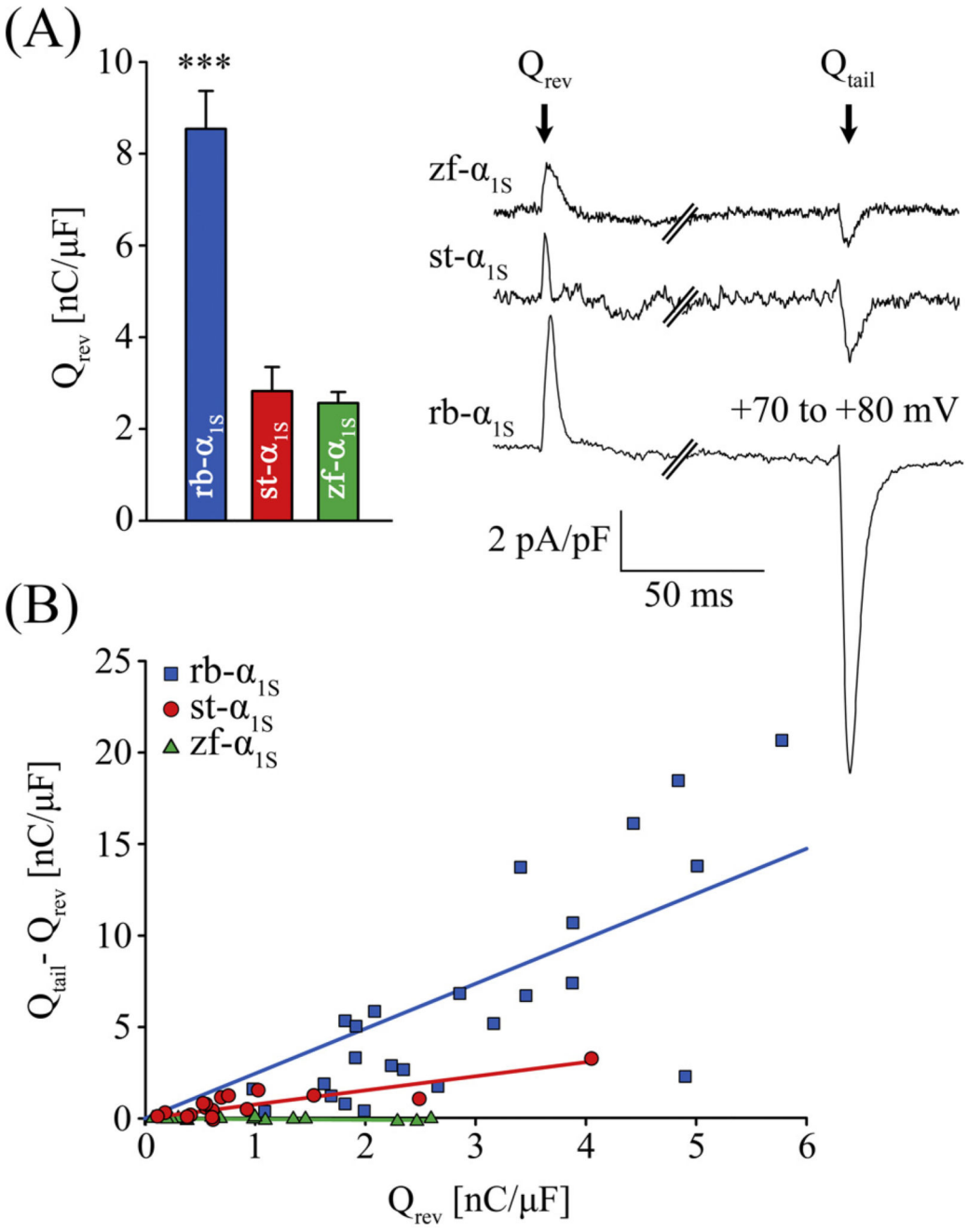

Fig. 3.

Reduced DHPR membrane expression and channel open probability in sterlet skeletal muscle. (A) Charge movement recordings at reversal potential (Q_{rev}) from GLT myotubes expressing rb-α_{1S} (blue bar; n = 24), st-α_{1S} (red bar; n = 17), or zf-α_{1S} (green bar; n = 21) indicated significantly lower ($p < 0.001$) membrane expression of both fish DHPRs. Representative charge movement traces are depicted on the right. Q_{rev} (indicated by the left arrow) is evaluated by integrating the area under the peak, induced by applying a 200-ms test potential at the reversal potential of +70 or +80 mV. (B) Relative DHPR open probability

(P_o) was calculated by plotting Q_{rev} versus [Q_{tail}− Q_{rev}] and comparing the slopes of the regression lines. Q_{tail} (indicated by the right arrow in A, right panel) is calculated by integrating the area under the tail current occurring at the end of the 200-ms test potential. P_o of st-α_{1S} (red circles) is significantly smaller ($p < 0.01$) than of rb-α_{1S} (blue squares). As expected, expression of zf-α_{1S} in GLT myotubes (green diamonds) displayed no conductance and thus the slope of the regression line was around zero, significantly different ($p < 0.001$) to sterlet and rabbit DHPRs. (For interpretation of the references to colour in this figure legend, the reader is referred to the web version of this article.)

Europe PMC Funders Author Manuscripts

Europe PMC Funders Author Manuscripts

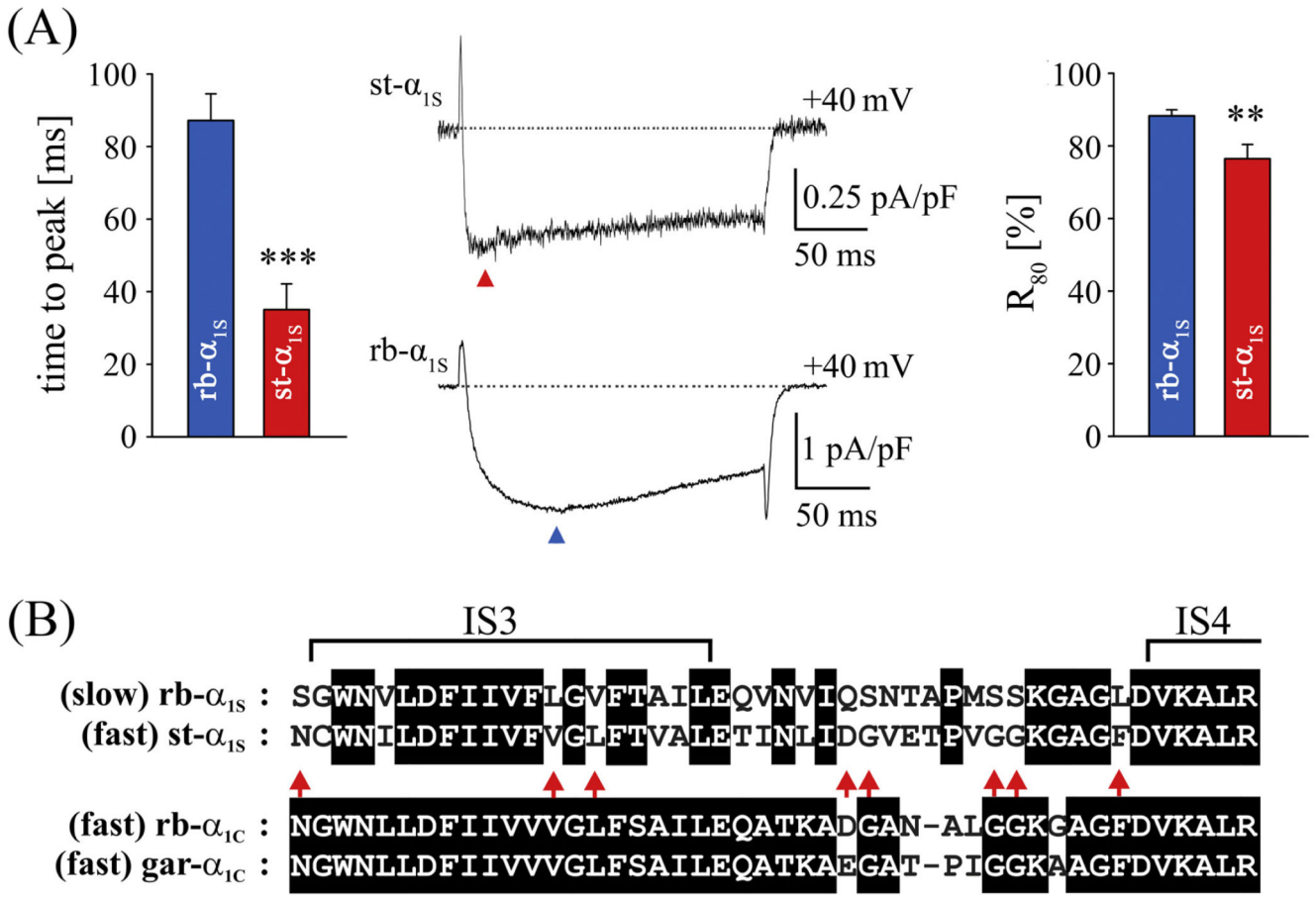

Fig. 4.

DHPR Ca^{2+} currents activate and inactivate faster in sterlet than in rabbit skeletal muscle. (A) (Left panel): DHPR Ca^{2+} currents peak significantly faster ($p < 0.001$) in st-α_{1S} (red bar; n = 20) compared to rb-α_{1S} (blue bar; n = 30) expressing GLT myotubes. (Middle panel): Representative traces of maximum DHPR current (I_{max}) at +40 mV test potential. The red arrowhead indicates the peak of sterlet I_{max} and the blue arrowhead of rabbit I_{max}. (Right panel): Analyses of fractional inactivation, 80 ms after the current peak (R_{80}) indicates acceleration of inactivation of sterlet DHPR currents compared to ($p < 0.01$) rabbit. (B) Amino acid sequence alignment of transmembrane segment IS3 and the adjacent IS3-IS4 linker (upper panel) known to be responsible for determining slow or fast activation of the DHPR current [36,37] revealed 19 amino acid exchanges (unboxed letters) between the slow activating rb-α_{1S} and the fast activating st-α_{1S}. Amino acid sequence alignment of fast activating cardiac DHPRs of rabbit and garfish (lower panel), revealed 8 amino acids to be identical to corresponding st-α_{1S} positions (red arrows). (For interpretation of the references to colour in this figure legend, the reader is referred to the web version of this article.)

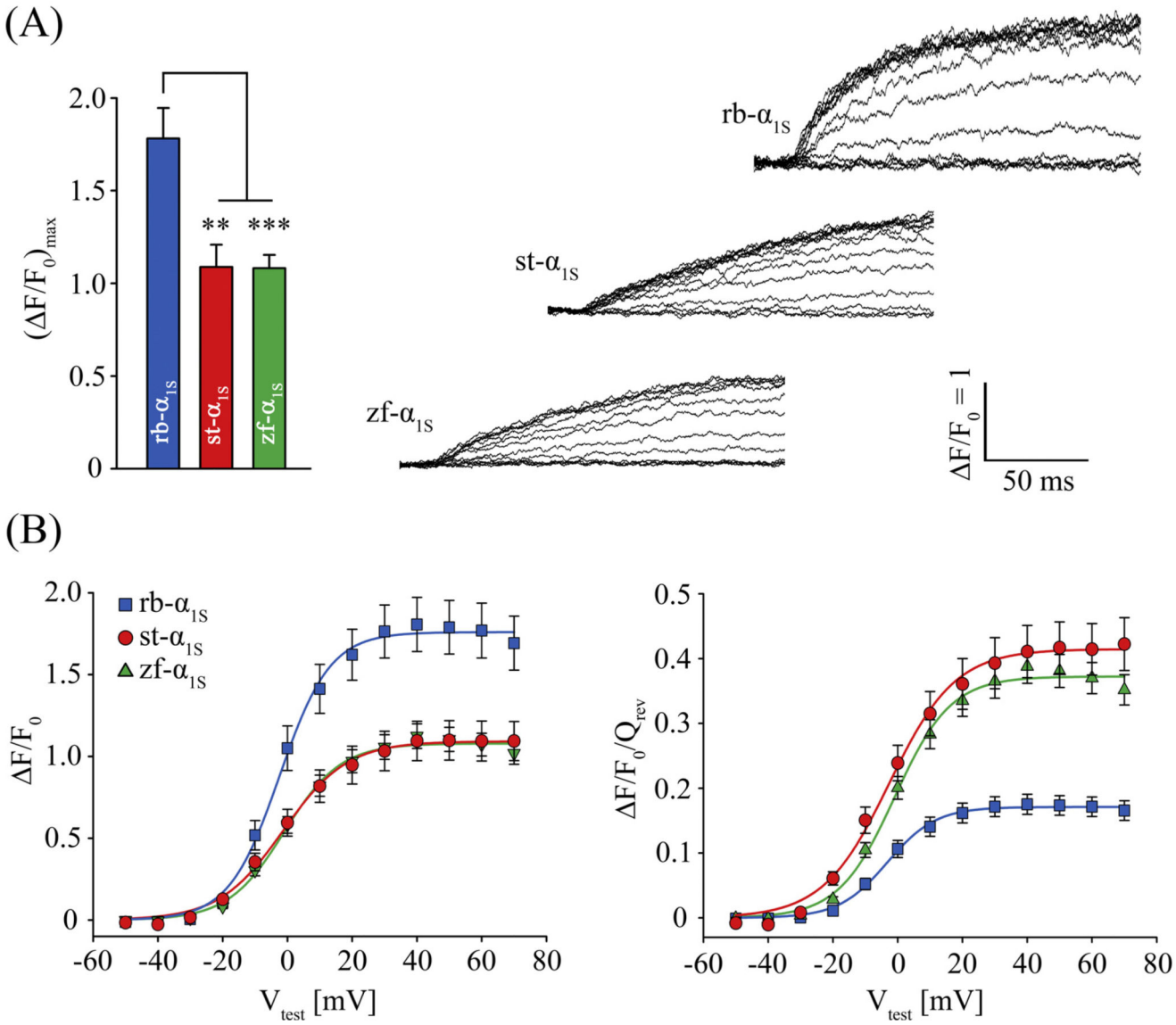

Fig. 5.

Reduced SR Ca^{2+} release but higher DHPR-RyR1 coupling efficacy in sterlet and zebrafish DHPRs. (A) GLT myotubes transfected with st-α_{1S} (red bar; n = 23) or zf-α_{1S} (green bar; n = 52) displayed significantly smaller maximal SR Ca^{2+} release ($(\Delta F/F_0)_{max}$) compared to ($p < 0.01$ and $p < 0.001$, respectively) rb-α_{1S}-expressing myotubes (blue bar; n = 39). Representative SR Ca^{2+} release traces are depicted on the right. (B) Voltage dependence of SR Ca^{2+} release shows identical ($p > 0.05$) half-maximum activation for all the three DHPRs. Comparison of the absolute voltage-dependence of Ca^{2+} release (left graphs) to the Ca^{2+} release normalized to DHPR expression levels (measured as Q_{rev}; right graphs) indicated significantly higher ($p < 0.001$) DHPR-RyR1 coupling efficacy in sterlet and zebrafish skeletal muscle compared to rabbit. (For interpretation of the references to colour in this figure legend, the reader is referred to the web version of this article.)

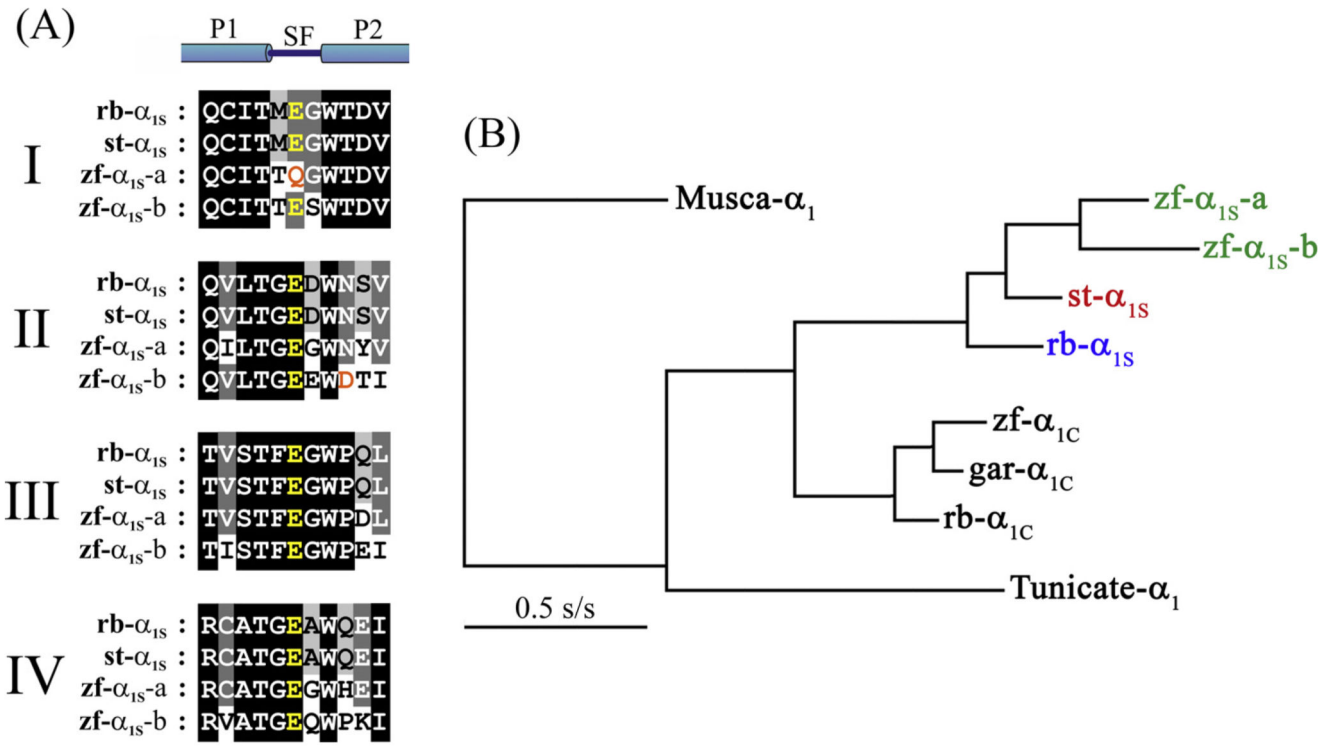

Fig. 6.

The phylogenetic position of the sterlet α_{1S} subunit. (A) Alignment of amino acid sequences forming and framing the DHPR Ca^{2+} selectivity filter of rb-α_{1S}, st-α_{1S}, zf-α_{1S}-a, and zf-α_{1S}-b. Pore loops I–IV (*I, II, III, IV*) are aligned and the critical EEEE residues of the Ca^{2+} selectivity filter are shown in *yellow*. The *blue rods* on top indicate the position of the two pore helices, P1 and P2 and the *blue line* indicates the selectivity filter vestibule (SF) [65]. The critical exchange of the selectivity filter glutamate (E303Q) in pore loop I of zf-α_{1S}-a, as well as the amino acid substitution N636D in pore loop II of zf-α_{1S}-b are indicated in *red*. Both these substitutions led to DHPR Ca^{2+} non-conductivity [18]. Amino acid exchanges are indicated as unboxed letters. (B) Phylogenetic tree based on parsimony analysis of full-length amino acid sequence alignments of rb-α_{1S}, st-α_{1S}, zf-α_{1S}-a and zf-α_{1S}-b, as well as cardiac DHPR counterparts including the garfish isoform (gar-α_{1C}; see Results). Ancestral DHPR isoforms from housefly (Musca-α_1) and tunicate (Tunicate-α_1) were used as outgroups. In both, the DHPRα_{1S} as well as DHPRα_{1C} cluster, rabbit isoforms are the most ancestral. Scale bar indicates evolutionary distance in substitutions per site (s/s). (For interpretation of the references to colour in this figure legend, the reader is referred to the web version of this article.)